Jurnal Teknologi

Full Paper

A COMPARATIVE STUDY OF PLA-ABS SANDWICH STRUCTURES: EFFECT OF PROCESS PARAMETERS ON MECHANICAL PERFORMANCES AND ENERGY CONSUMPTION

Andri Nasution[a,b]; Sarah Iftin Atsani[c]; Hasan Mastrisiswadi[a,d], Achmad Pratama Rifai[a]; Herianto[a*]

[a]Department of Mechanical and Industrial Engineering, Universitas Gadjah Mada, Yogyakarta 55281, Indonesia
[b]Department of Industrial Engineering, Universitas Sumatera Utara, Medan 20155, Indonesia
[c]Center of Additive Manufacturing and Systems, Yogyakarta 55281, Indonesia
[d]Department of Industrial Engineering, UPN Veteran Yogyakarta, Yogyakarta 55281, Indonesia

Article history
Received
8 December 2024
Received in revised form
13 May 2025
Accepted
13 May 2025
Published Online
27 February 2026

*Corresponding author
herianto@ugm.ac.id

Graphical abstract

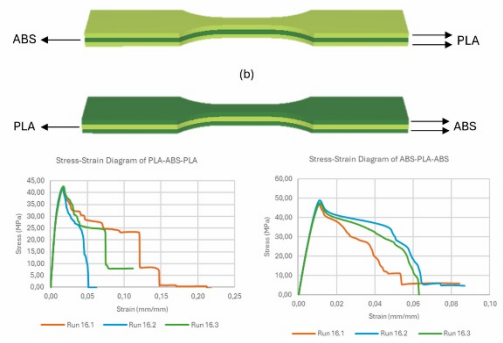

Abstract

Additive manufacturing (AM) is increasingly recognized as a sustainable technology due to its ability to minimize material usage, reduce waste, offer flexibility, and decrease the need for mass production. However, energy consumption during the processing phase raises sustainability concerns. While previous research has examined the impact of process parameters on energy consumption, most studies have been limited to single-material and single-nozzle configurations. On the other hand, the growing advancement towards the integration of multiple materials in AM warranting further investigation in multi-material context. This study addresses these gaps by investigating the effects of various process parameters in multi-material FDM printing on energy consumption, build time, dimensional accuracy, and tensile strength, focusing on two multi-material sandwich structures: PLA/ABS/PLA (PAP) and ABS/PLA/ABS (APA). The results indicate that the APA structure generally exhibits superior tensile strength, but lower dimensional accuracy compared to the PAP structure, although it consumes more energy despite variations in build time. When compared to existing literature, both structures outperform standard ABS and PLA in several key mechanical properties. Data analysis reveals a clear positive correlation between build time and energy consumption but no strong correlation between tensile strength and either build time or energy consumption. ANOVA analysis further identifies significant process parameters affecting the four key metrics, with variations observed between the PAP and APA structures. These findings underscore the importance of selecting appropriate process parameters in multi-material FDM printing to optimize both performance and sustainability.

Keywords: Fused deposition modelling; Multi nozzle 3D printing; Multi material; Energy consumption; Tensile properties

1.0 INTRODUCTION

Additive manufacturing (AM), commonly known as 3D printing, is a process of creating objects by sequentially adding material layer by layer, based on a digital model [1]. It enables the creation of intricate and customized designs that would be difficult or impossible to achieve with conventional methods [2]. In 2011, the global revenue for AM goods reached approximately $642.6 million [3], with widespread application across industries such as aerospace, automotive, healthcare, and consumer goods. Current AM developments on improving speed, precision, and the range of materials are driving the market value towards an estimated $50 billion by 2030 [3]. This significant growth in AM underscores the critical importance of researching its sustainability.

Owing to some key factors, AM can be considered a sustainable technology. Firstly, it minimizes material usage by adding material layer by layer only where needed, which significantly reduces waste production compared to conventional subtractive manufacturing methods [4]. Additionally, the precision of AM reduces the need for excess raw material, lowering both environmental impact and costs [5]. Secondly, AM enables the production of customized batches tailored to specific customer requirements, enhancing flexibility and reducing the necessity for mass production and large inventories [6]. This adaptability allows companies to respond swiftly to market demands, decreasing overproduction and the associated waste. Moreover, AM facilitates the rapid and cost-effective creation of prototypes [7]. This capability accelerates the time-to-market for new products, enabling faster innovation cycles and reducing the resources spent on prolonged development phases [8].

However, despite its substantial benefits, AM also raises sustainability-related concerns. One significant concern is the energy consumption during the processing phase of AM [9]. This technology often requires considerable energy inputs for heating, melting, and solidifying materials, which can contribute to a higher carbon footprint compared to conventional manufacturing processes [10]. Another critical concern relates to the strength and reliability of the 3D printed parts. While AM allows for intricate designs and customization, it exhibits anisotropic behaviour due to the layer-by-layer printing process [11]. This results in varying microstructures between layers, affecting the mechanical properties of the printed parts [12]. Such behaviour can diminish the performance and longevity of parts in real-world applications, particularly in applications requiring consistent and reliable mechanical strength across all orientations.

Fused Deposition Modelling (FDM) is one of the most commonly employed AM techniques. FDM technology accounts for a significant portion of the global additive manufacturing market, with estimates indicating it constituted around 40% of all 3D printing system market worldwide in recent years [13]. This method is popular for several reasons. Firstly, FDM is relatively affordable and accessible compared to other AM technologies [14], making it feasible for a wide range of users, from small businesses to large corporations. Secondly, FDM offers versatility in material choices [15], allowing manufacturers to work with a variety of thermoplastics suitable for different applications. Additionally, FDM's simple workflow and ease of use [16] make it suitable for rapid prototyping, low-volume production, and even custom manufacturing, providing flexibility and efficiency in product development cycles.

Numerous studies have been undertaken to address and improve the mechanical properties of FDM-printed parts. One well-known approach is to adjust the printing parameters. Various parameters have been explored for their influence on mechanical properties in FDM-printed components including print speed, layer thickness, extrusion temperature, infill pattern and density, nozzle diameter, build orientation, layer adhesion, and cooling rate. For instances, smaller layer thickness generally results in stronger parts due to improved interlayer bonding [17], [18], [19], while smaller infill density results in weaker parts due to airgap between layers [20], [21], [22].

Some researchers have also examined the combined effects of multiple printing parameters to optimize the FDM process. Specifically, in the study by Rarani et.al [23] found that the optimal combination of parameters to achieve the highest tensile strength of Polylactic Acid (PLA) FDM-printed parts includes print speed of 40 mm/s, infill density of 80%, and layer thickness of 0.1 mm. Meanwhile the study by Srinivasan et.al [24] predicts that the optimal setup for Acrylonitrile Butadiene Styrene (ABS) to achieve the desirable tensile strength was triangular infill pattern, infill density of 80%, and layer thickness of 0.1 mm. These studies have provided valuable insights into how different factors interact to influence tensile properties.

Another approach to enhance the mechanical strength of FDM-printed parts is through material combinations. The advancement of AM towards the integration of multiple materials is significantly enhancing the capabilities and advantages of AM in product fabrication. Among the various techniques, FDM which categorized as Material Extrusion (ME) stands out as the most accessible and straightforward method for implementing multi-material applications, offering greater flexibility and innovation in the design and production process. Rasheed *et al*. [25] have investigated the use of FDM for fabricating multi-material components composed of PLA and ABS. Their findings indicated that the sandwich structure of ABS-PLA layers exhibited higher tensile strength compared to parts made solely of ABS. Similarly, Baca *et al*. [26] examined how combining different sections of a part using three materials—ABS, PLA, and High Impact Polystyrene (HIPS)—impacted mechanical properties. They discovered that incorporating ABS or PLA into HIPS parts resulted in increased tensile strength compared to using only HIPS. Yadav *et al*. [27] also explored the optimization of mechanical properties in FDM-printed parts by using a multi-material approach with ABS and

Polyethylene Terephthalate Glycol (PETG). Their research demonstrated that the tensile strength of ABS-PETG sandwich structures was superior to that of parts made from ABS alone.

In terms of energy consumption in FDM, it can be categorized into two main categories including primary energy which is the thermal energy needed to melt the filament, and secondary energy that encompasses the power required for mechanical movements and maintaining auxiliary temperature fields [28]. In practices, the total energy consumption for an FDM process is estimated to be around 1,220.8 kJ [29]. Notably, the build plate alone accounts for more than half of the total energy used during the printing process [30].

Some researchers have also investigated how process parameters impact energy consumption in FDM printing. Negrete's [31] experimental study explored the optimization of printing time, energy usage, and dimensional accuracy of FDM-printed parts by adjusting five parameters such as layer thickness, infill pattern, build orientation, printing plane, and part positioning. Lunetto *et al*. [32] focused on the effect of layer thickness and infill strategy on both production time and consumed energy. Enemuoh *et al*. [33] quantified the impact of printing parameters such as infill density, infill pattern, print speed, layer thickness, and shell thickness on a range of outcomes. They studied how these factors influenced mass of part, dimensional accuracy, processing time, energy consumption, hardness, and tensile strength.

Those previous studies collectively have offered a detailed understanding of how to balance various printing parameters to optimize energy efficiency and part quality. However, the studies often focus on single-material and single-nozzle configurations. This study aims to address these gaps by investigating the effects of various process parameters in multi-material FDM printing on energy consumption. An experimental approach is used, combining ABS and PLA materials. The process parameters explored include layer thickness, raster width, raster angle, print speed, build orientation, infill density, material composition, nozzle temperature, and bed temperature. In addition to energy consumption, the study examines how these parameters affect build time, dimensional accuracy, and mechanical properties such as tensile strength. Finally, the comparison in this study will provide a more holistic understanding of the interplay between printing parameters, energy consumption, and part quality in multi-material FDM printing.

2.0 MATERIALS AND METHODOLOGY

2.1 Material Composition

In this research, a sandwich structure was used to form specimens. There were three main layers of material arranged in either a PLA-ABS-PLA (PAP) or ABS-PLA-ABS (APA) sequence (Figure 1). The composition of these materials is a critical parameter in the study, with specific ratios of PLA and ABS being tested. The material compositions used include 35/30/35; 25/50/25; and 15/70/15. For instance, in the PAP structure with a 35/30/35 composition, means that 35% represents the PLA layer in contact with the bed, 30% corresponds to the ABS layer following the PLA, and the final 35% refers to the top PLA layer positioned above the ABS. These varying proportions were designed to investigate the impact of different PLA and ABS ratios on the final properties of the specimens.

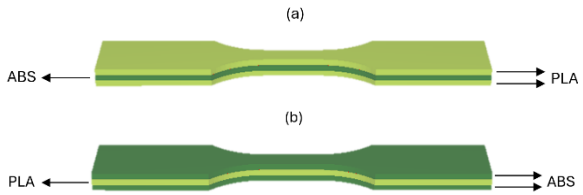

Figure 1 Material compositions: (a) PLA-ABS-PLA; (b) ABS-PLA-ABS

2.2 Design of Experiment

Design of experiment used Taguchi method with L27 orthogonal array, each configuration repeated five times. In this study, the L27 orthogonal array accommodates seven factors with 3 levels of parameter as detailed in Table 1. Other process parameters listed in Table 2 remain consistent across all experiments. The observed output was the tensile strength, build time, dimensional accuracy, and energy consumption.

Table 1 Observed process parameter

Input Parameter	Unit	Level		
		1	2	3
Layer thickness	mm	0.2286	0.2540	0.3302
Raster angle	°	0	45	90
Build orientation	°	0	30	45
Raster width	mm	0.484	0.520	0.578
Speed	mm/s	40	50	60
Infill Density	%	80	90	100
Material composition	%	15/70/15	25/50/25	35/30/35

The selection of parameter values in this study is guided by findings from previous literature to optimize mechanical performance and manufacturing efficiency. For layer thickness, the range of 0.17–0.33 mm was identified by Giri *et al*. [34] as effective in maximizing tensile strength while minimizing build time. A specific value of 0.2286 mm has been reported by Poonia *et al*. [35] and Rojek *et al*. [36] to be optimal for dimensional accuracy and tensile strength stability. Additionally, in [37], [38], [39], [40], they found that a thickness of 0.2540 mm offers a favorable balance between tensile strength and build time. Mohamed *et*

al's [41] study further indicated that a thickness of 0.3302 mm provides improvements in dimensional accuracy, build time, and energy consumption.

For the raster angle, values of 0°, 45°, and 90° were chosen based on studies conducted by [34], [39], [41], [42] which demonstrated these angles to be effective in enhancing tensile strength. Similarly, build orientation values (0°, 30°, 45°) were adopted from previous studies ([34], [37], [38], [39], [40], [41], [42]) that investigated a similar range of parameters, with the 0° orientation shown to deliver the best results in terms of tensile strength and build efficiency.

Regarding raster width, some studies identified 0.484 mm as optimal for reducing build time and enhancing tensile strength [38], [40], [41]. Sood *et al*. [39] supported a raster width of 0.520 mm for its positive impact on tensile strength, while Mohamed *et al*. [41] found that 0.578 mm contributes to an increase in the storage modulus. For printing speed, values of 40, 50, and 60 mm/s were selected based on investigations by [36], [43], [44], all of whom found these speeds beneficial for tensile strength.

The infill density values of 80%, 90%, and 100% were selected in accordance with studies by [45], [46], [47], [48]. These studies concluded that higher infill densities improve tensile strength and Young's modulus while also reducing build time and energy consumption.

In contrast, material composition remains a relatively unexplored parameter. Only Baca *et al*. [46] have investigated a composition ratio of 35/30/35. To address this gap, the present study introduces two additional composition ratios to further explore their influence on mechanical and process-related outcomes.

Table 2 Fixed process parameter

Parameter	Material composition	
	PLA/ABS/PLA	ABS/PLA/ABS
Nozzle Temperature (°C)	210/250/210	250/210/250
Wall line count	2	
Line width (mm)	0.484	
Bed Temperature (°C)	60	90
Infill Pattern	Line	
Fan Speed (mm/s)	100	
Travel Speed (mm/s)	120	

2.3 Tensile Test

The specimen was prepared according to the ASTM D638-14 type V standard, which specifies the dimensions and shape required for tensile testing as illustrated in Figure 2. The ASTM D638-14 Type V specimen was selected due to its smaller size, which is more compatible with the limited build volume of desktop multimaterial printers. Additionally, Type V is widely adopted in FDM-related studies to evaluate the tensile properties of composites within constrained geometries, for example in [49], [50], [51], [52]. The tensile tests were conducted using a Tensilon RTI-1225 testing machine. During the tests, the specimen was securely clamped and subjected to a continuously increasing load until it ultimately broke.

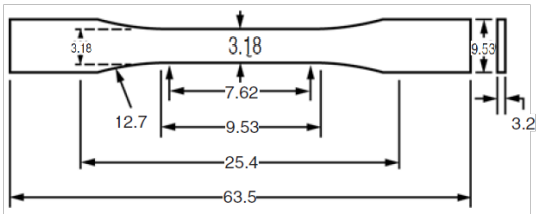

Figure 2 ASTM D638-14 type V for tensile strength (dimension in mm)

2.4 Dimensional Accuracy

A digital calliper was used to measure the dimensions of the specimens including length, width and thickness. After that, the actual measurement results were compared with the CAD specimen dimension. Dimensional accuracy units were expressed in percentage (%).

2.5 Build Time

Build time was measured straightforwardly with a digital stopwatch. The measurement begins as soon as the 3D printing machine starts printing the specimen and stops the moment the machine finishes the print. The total time taken for the printing process was then recorded in seconds (s).

2.6 Energy Consumption

Energy consumption was measured using a watt meter. The measurement starts when the 3D printing machine begins the printing process and ends when the machine finishes printing. The total electrical energy required was recorded in kWh.

2.7 Data Processing

Data processing was performed using Taguchi analysis to determine the optimal combination of factors that affect the outcome. Following this, ANOVA (Analysis of Variance) was used to identify the factors that have a significant impact on the results.

3.0 RESULTS AND DISCUSSION

Table 3 presents the measurement results for tensile strength, dimensional accuracy, build time, and energy consumption for two printing structures: PLA-ABS-PLA (PAP) and ABS-PLA-ABS (APA). The results shown are the average values obtained from five repetitions for each parameter. The data reveals that the APA structure generally exhibits higher tensile strength compared to the PAP structure, with exceptions noted in runs 4 and 1. On the contrary, PAP shows better dimensional accuracy than APA. Despite the varying build times, APA tends to consume more energy compared to PAP.

Specifically, in runs 1, 4, 5, 7, 9, 10, 15, 16, 17, 24, and 27, APA's build time is shorter than PAP's, yet it still uses more energy. This can be attributed to the higher nozzle and bed temperatures required for printing the APA structure compared to the PAP structure, which in turn demands more energy.

The standard deviation values for the measurement results are presented separately in Table 4. Upon review, it is evident that the data for tensile strength, dimensional accuracy, and energy consumption exhibit very low standard deviations, all less than 2. This small standard deviation indicates that the data points are tightly clustered around the mean, suggesting a high degree of consistency and minimal variability across the samples. In contrast, the standard deviation for build time ranges from 0.4 to 29.96. This broader range of variability in build time can be attributed to several factors during the printing process. Specifically, some specimens required over 200 seconds more than others to complete.

Table 3 Experiment results

No. Run	Process Parameters							Tensile Strength (MPa)		Dimensional Accuracy (%)		Build Time (s)		Energy Consumption (kWh)	
	Layer Thickness	Raster Angle	Build Orientation	Raster Width	Speed	Infill Density	Composition	PAP	APA	PAP	APA	PAP	APA	PAP	APA
1	0.229	0	0	0.484	40	80	35/30/35	32.05	36.31	99,20%	98,45%	481.2	472.0	0.0186	0.0334
2	0.229	0	0	0.484	50	90	25/50/25	38.76	45.12	98,52%	97,29%	467.0	474.4	0.0180	0.0348
3	0.229	0	0	0.484	60	100	15/70/15	37.13	42.79	98,89%	95,81%	482.0	482.8	0.0190	0.0368
4	0.229	45	30	0.520	40	80	35/30/35	42.73	41.95	99,52%	98,48%	422.4	412.8	0.0154	0.0290
5	0.229	45	30	0.520	50	90	25/50/25	41.09	46.14	98,85%	97,65%	404.0	401.0	0.0154	0.0292
6	0.229	45	30	0.520	60	100	15/70/15	35.83	42.16	99,06%	96,54%	395.2	397.0	0.0150	0.0298
7	0.229	90	45	0.578	40	80	35/30/35	40.17	42.18	99,44%	98,41%	404.0	402.0	0.0146	0.0298
8	0.229	90	45	0.578	50	90	25/50/25	42.22	44.40	98,90%	96,14%	385.8	396.8	0.0152	0.0318
9	0.229	90	45	0.578	60	100	15/70/15	38.57	43.14	98,87%	95,41%	393.6	391.6	0.0158	0.0310
10	0.254	0	30	0.578	40	90	15/70/15	42.39	47.13	98,34%	95,21%	414.4	413.8	0.0168	0.0324
11	0.254	0	30	0.578	50	100	35/30/35	39.71	42.37	98,63%	96,48%	378.0	381.0	0.0152	0.0288
12	0.254	0	30	0.578	60	80	25/50/25	36.67	42.35	98,35%	97,32%	342.6	348.8	0.0144	0.0264
13	0.254	45	45	0.484	40	90	15/70/15	40.69	45.56	98,34%	96,16%	416.0	427.2	0.0174	0.0326
14	0.254	45	45	0.484	50	100	35/30/35	37.04	42.31	98,48%	95,53%	394.8	397.6	0.0162	0.0284
15	0.254	45	45	0.484	60	80	25/50/25	42.01	41.89	99,30%	96,64%	350.0	348.2	0.0138	0.0262
16	0.254	90	0	0.520	40	90	15/70/15	44.36	47.57	98,79%	95,70%	398.8	395.8	0.0158	0.0302
17	0.254	90	0	0.520	50	100	35/30/35	40.65	43.48	99,08%	95,39%	356.2	346.0	0.0132	0.0254
18	0.254	90	0	0.520	60	80	25/50/25	39.27	46.18	98,92%	97,40%	307.2	309.0	0.0120	0.0236
19	0.330	0	45	0.520	40	100	25/50/25	39.90	40.75	98,44%	95,91%	345.4	350.4	0.0142	0.0260
20	0.330	0	45	0.520	50	80	15/70/15	33.94	43.02	99,32%	96,88%	314.0	320.0	0.0124	0.0240
21	0.330	0	45	0.520	60	90	35/30/35	38.20	40.67	98,42%	97,75%	308.4	310.0	0.0114	0.0224
22	0.330	45	0	0.578	40	100	25/50/25	36.69	44.00	99,03%	96,85%	319.0	322.4	0.0118	0.0234
23	0.330	45	0	0.578	50	80	15/70/15	37.25	43.88	99,30%	96,65%	304.8	304.8	0.0116	0.0232
24	0.330	45	0	0.578	60	90	35/30/35	33.04	39.52	98,88%	98,30%	281.4	271.6	0.0110	0.0194
25	0.330	90	30	0.484	40	100	25/50/25	37.48	38.74	99,15%	96,12%	346.0	362.8	0.0138	0.0276
26	0.330	90	30	0.484	50	80	15/70/15	33.52	41.74	99,18%	96,76%	313.6	329.4	0.0122	0.0254
27	0.330	90	30	0.484	60	90	35/30/35	37.97	38.91	98,97%	97,31%	312.4	307.0	0.0118	0.0234

Table 4 Standard Deviation

No Run	Tensile		Dimentional Accuracy		Build Time		Energy Consumption	
	PAP	APA	PAP	APA	PAP	APA	PAP	APA
1	1.55	0.89	0.00	0.00	6.61	2.35	0.00	0.00
2	0.55	0.69	0.01	0.01	7.31	0.55	0.00	0.00
3	0.64	0.66	0.00	0.01	5.66	6.06	0.00	0.00
4	0.18	0.25	0.00	0.01	6.95	5.85	0.00	0.00
5	0.24	0.28	0.01	0.01	12.31	10.77	0.00	0.00
6	0.26	0.59	0.00	0.00	7.43	7.42	0.00	0.00
7	0.79	0.37	0.00	0.01	6.44	11.07	0.00	0.00
8	0.40	0.51	0.01	0.01	6.06	7.60	0.00	0.00
9	0.91	0.05	0.00	0.01	11.50	1.14	0.00	0.00
10	0.26	0.13	0.00	0.01	1.14	5.59	0.00	0.00
11	0.35	0.26	0.00	0.00	6.89	6.16	0.00	0.00
12	0.81	0.57	0.00	0.00	11.55	5.72	0.00	0.00
13	0.34	0.36	0.00	0.01	11.36	7.40	0.00	0.00
14	0.75	0.82	0.01	0.01	9.55	11.97	0.00	0.00
15	0.21	0.88	0.00	0.01	9.19	0.45	0.00	0.00
16	0.13	0.31	0.01	0.01	5.72	6.94	0.00	0.00
17	0.57	0.33	0.00	0.01	7.12	11.77	0.00	0.00
18	0.36	0.23	0.00	0.01	29.96	5.15	0.00	0.00
19	0.29	0.51	0.00	0.00	7.67	1.14	0.00	0.00
20	1.00	0.65	0.00	0.00	7.14	5.83	0.00	0.00
21	1.24	0.73	0.01	0.00	5.86	15.98	0.00	0.00
22	0.38	0.35	0.00	0.00	6.00	6.43	0.00	0.00
23	0.59	0.25	0.01	0.00	18.86	8.70	0.00	0.00
24	1.02	0.55	0.00	0.01	5.94	7.23	0.00	0.00
25	0.25	0.62	0.01	0.02	7.31	5.22	0.00	0.00
26	0.40	0.80	0.00	0.01	10.92	7.99	0.00	0.00
27	0.47	1.10	0.00	0.01	6.77	6.16	0.00	0.00

No Run	Tensile		Dimentional Accuracy		Build Time		Energy Consumption	
	PAP	APA	PAP	APA	PAP	APA	PAP	APA
Minimum	0.13	0.05	0.00	0.00	1.14	0.45	0.00	0.00
Maximum	1.55	1.10	0.01	0.02	29.96	15.98	0.00	0.00

3.1 Tensile Properties of Multi-Material Structure

Based on the results in Table 3, the highest tensile strength for both PAP and APA structures is observed in Run 16. To validate these results, three additional specimens of each structure were prepared with process parameters in Run 16 and subjected to tensile testing. Figure 3 illustrates the stress-strain curve, while Table 5 provides the tensile properties for three repetitions of PAP and APA in Run 16. From the data, The APA structure consistently demonstrates superior mechanical properties in terms of Ultimate Tensile Strength (UTS), yield strength, and Young's modulus compared to the PAP structure, indicating its potential for applications requiring higher strength and stiffness. However, the PAP structure shows greater elongation at break, suggesting better ductility and the ability to withstand more strain before failure, which might be beneficial in applications where flexibility is crucial.

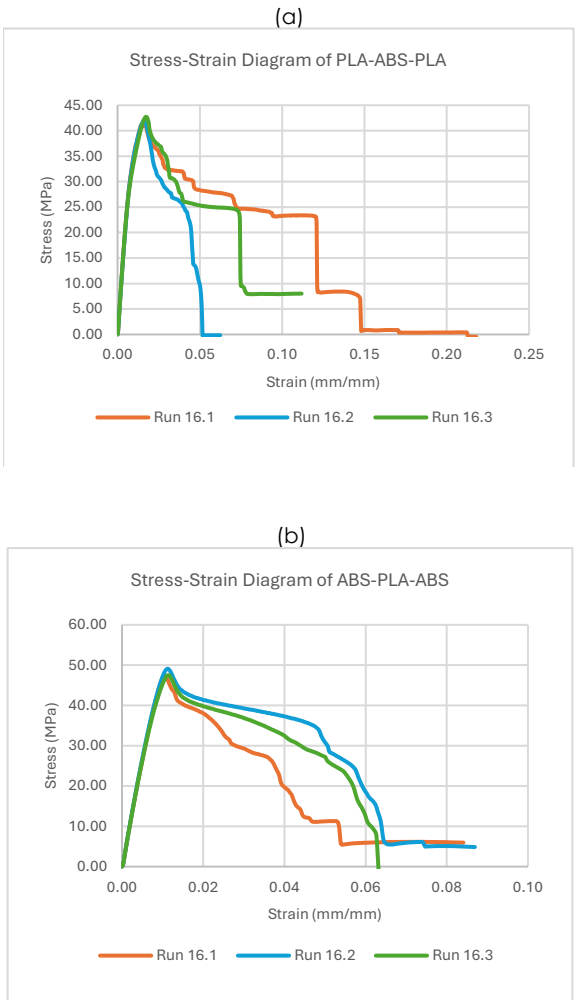

Figure 3 Stress-elongation curve of: (a) PAP; and (b) APA specimens in Run 16

In this study, control samples consisting of single PLA and single ABS were also prepared by printing three specimens for each material using the process parameters from Run 16, as detailed in Table 6. Based on the data presented in Table 5, the average UTS for the PAP structure is 42.07 MPa, while the APA structure exhibits a higher average UTS of 48.03 MPa. Both the PAP and APA structures demonstrate superior UTS values when compared to the single PLA and single ABS samples, which have average UTS values of 17.12 MPa and 24.82 MPa, respectively, as shown in Table 6. Furthermore, the APA structure exhibits a UTS that exceeds the highest UTS reported for ABS in the studies by Bernadez et.al (35.2 MPa) [53], Panda et.al (18.09 MPa) [38], Fountas et.al (35.90 MPa) [54], and Baca et.al (32.9 MPa) [26]. The PAP structure's UTS is also higher than the UTS reported for PLA in studies by Kam et.al (38.92 MPa) [55] and Kananathan et.al (37.5 MPa) [56], but slightly lower than the highest UTS for PLA reported in Baca et.al's study (47.5 MPa) [26]. This suggests that multi-material structures enhance the strength compared to what can be achieved with a single material.

Table 5 Tensile properties of PAP and APA specimens in Run 16.

Material Composition	Repetition	Ultimate Tensile Strength (MPa)	Yield Strength (MPa)	Young's Modulus (MPa)	Elongation at break (%)
PLA-ABS-PLA (PAP)	1	41.44	36.29	4116.0	21.80
	2	42.03	36.04	4238.7	6.24
	3	42.72	34.51	4214.1	11.18
	AVG	42.07	35.61	4189.6	13.07
ABS-PLA-ABS (APA)	1	42.48	45.88	4855.9	8.41
	2	49.09	47.99	4915.8	8.69
	3	47.52	47.515	4733.5	7.06
	AVG	48.03	47.19	4835.1	8.05

Table 6 Tensile test of control samples

Parameters in Run	Material Composition	Repetition	UTS (MPa)	Average UTS (MPa)
16	Single ABS	1	23.69	24.81
		2	27.04	
		3	23.69	
	Single PLA	1	11.64	17.12
		2	18.97	
		3	20.75	

The average yield strength of the PAP structure is 35.61 MPa, whereas for the APA structure, it is significantly higher at 47.19 MPa. The yield strength of APA and PAP exceeds the highest yield strength of single material PLA reported in Kananathan et.al's study (23.33 MPa) [56], indicating superior performance of multi-material structures in terms of resistance to deformation.

The Young's modulus for the PAP structure is 4189.6 MPa, and for the APA structure, it is 4835.1 MPa. Both PAP and APA structures have significantly higher

Young's modulus values compared to those reported for ABS in Bernadez et.al (795.9 MPa) [53] and Baca et.al (1050 MPa) studies [26], and also exceed the Young's modulus values for PLA in Kananathan et.al (1147.76 MPa) [56] and Baca et.al (1397 MPa) studies [26]. This indicates that both multi-material structures are much stiffer than typical ABS or PLA alone.

The average elongation at break for the PAP structure is 13.07%, while for the APA structure, it is lower at 8.05%. The elongation at break for PAP and APA is significantly higher than the highest reported value for PLA and ABS in Baca et.al (4.6% and 5% respectively) [26] but significantly lower than the highest ABS elongation reported in Bernadez et.al's study (26%) [53]. The higher elongation at break for both multi-material structure indicates that they have better ductility compared to the single PLA and ABS in some literature.

3.2 Dimensional Accuracy

Based on the dimensional accuracy data for the PAP structure (Figure 4(a)) and APA structure (Figure 4(b)), several key observations and implications can be drawn. The dimensional accuracy values for both PAP and APA structures, considering Length, Width, and Thickness, are close to 100%, with the highest average accuracy recorded at approximately 99.52% for the PAP structure and 98.48% for the APA structure, both in Run 4. Conversely, the lowest average value was observed at 98.34% for PAP in Run 13 and 95.21% for APA in Run 10. These findings suggest that both structures generally maintain high dimensional accuracy, though some variation exists between different runs and across the different dimensions measured.

On average, the overall dimensional accuracy for the PAP structure (PLA-ABS-PLA) is higher than that of the APA structure (ABS-PLA-ABS). This discrepancy can be attributed to material properties and their behaviour during the 3D printing process. Different materials used in 3D printing can exhibit varying degrees of shrinkage or expansion during cooling or solidification, which in turn affects the final dimensional accuracy. Specifically, ABS material is known to be more susceptible to shrinkage compared to PLA [19]. This phenomenon is supported by Milde *et al*. [57], who found that ABS parts shrink more than PLA parts in terms of outer and inner distance deviation. The study revealed that components fabricated from ABS material experienced dimensional deviations of more than 0.34 mm on the outer surfaces in the X-axis, whereas the deviation for PLA components was less than 0.27 mm [57]. This material behaviour likely explains why the dimensional accuracy of the APA structure, which contains more ABS layer, is lower than that of the PAP structure.

The dimensional accuracy values for Length, Width, and Thickness measurements across all runs are generally consistent for both PAP and APA structures. However, a noticeable trend is the lower accuracy observed in the Thickness measurements compared to Length and Width. This discrepancy can be attributed to the inherent challenges in achieving high dimensional accuracy in the vertical (thickness) direction in 3D printing, which is often more difficult than achieving similar accuracy in the horizontal (length and width) dimensions.

One reason for this lower accuracy in Thickness could be the influence of layer height settings and printer resolution. In 3D printing, the precision of thickness measurements is largely affected by the layer height used during the printing process [58]. If the layer height is not fine enough, the resulting printed thickness may deviate from the intended value, leading to reduced dimensional accuracy [59]. Furthermore, 3D-printed structures often exhibit anisotropic properties, meaning that their mechanical and dimensional characteristics vary depending on the direction of printing [60]. In particular, thickness is influenced by the z-axis, where the layer-by-layer construction occurs, and this direction is often the least accurate in terms of both mechanical and dimensional properties. Consequently, the observed lower accuracy in Thickness may be a result of these inherent limitations in the 3D printing process, especially for complex geometries or components that rely on precision in the vertical dimension.

(a)

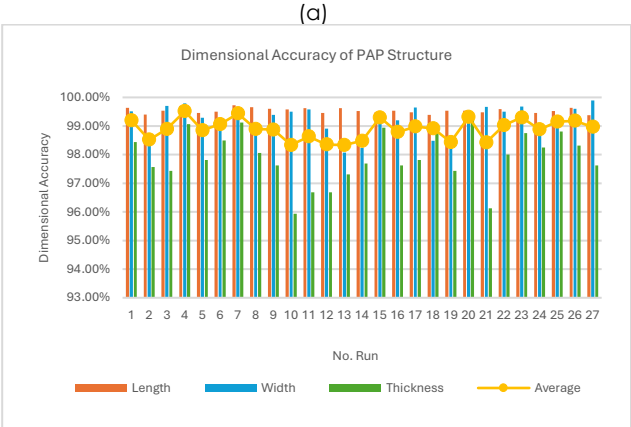

(b)

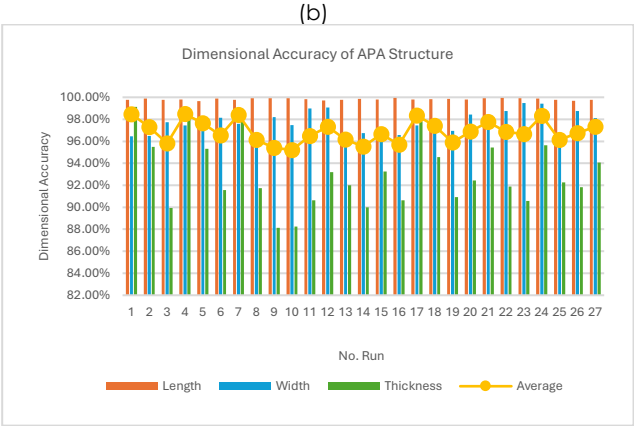

Figure 4 Dimensional accuracy of 3 axis in: (a) PAP; (b) APA structure.

3.3 Tensile strength VS build time

The data points in Figure 5 do not show a clear linear trend, indicating that there is no strong correlation between tensile strength and build time in both PAP and APA structure. The tensile strength values appear to be relatively dispersed across different build times, suggesting that build time might not be the primary factor influencing tensile strength.

For the PAP structure, the highest tensile strength recorded is 44.36 MPa, achieved with a build time of 398.8 seconds during Run 16. Conversely, the lowest tensile strength observed is 32.05 MPa, associated with a longer build time of 481.2 seconds in Run 1. The longest build time of 482.0 seconds, observed in Run 3, resulted in a tensile strength of 37.13 MPa, while the shortest build time of 281.4 seconds, observed in Run 24, yielded a tensile strength of 33.04 MPa.

Interestingly, the highest and lowest of tensile strengths and build time for APA occur in the same runs as that of PAP. The highest tensile strength recorded is 47.57 MPa, with a build time of 395.8 seconds in Run 16. The lowest tensile strength is 36.31 MPa, associated with a longer build time of 472.0 seconds in Run 1. The longest build time recorded is 482.8 seconds in Run 3, which resulted in a tensile strength of 42.79 MPa. Meanwhile, the shortest build time of 271.6 seconds, recorded in Run 24, produced a tensile strength of 39.52 MPa.

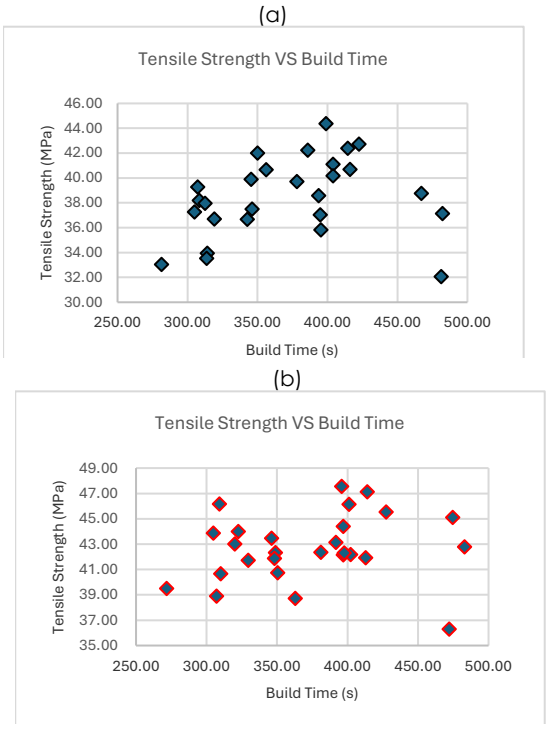

Figure 5 Tensile strength VS build time data plots of: (a) PAP structure; (b) APA structure.

3.4 Tensile strength VS energy consumption

Based on Figure 6 there does not appear to be a strong or clear correlation between tensile strength and energy consumption. The data points are scattered, indicating that energy consumption does not have a straightforward impact on tensile strength.

For the PAP structure, the highest tensile strength recorded is 44.36 MPa, corresponding to an energy consumption of 0.0158 kWh in Run 16. In contrast, the lowest tensile strength of 32.05 MPa is associated with a higher energy consumption of 0.0186 kWh in Run 1. The highest energy consumption recorded is 0.019 kWh in Run 3, which results in a tensile strength of 37.13 MPa. Conversely, the lowest energy consumption of 0.011 kWh, observed in Run 24, yields a tensile strength of 33.04 MPa.

The highest and lowest of tensile strengths and energy consumption for APA also happen in the same runs as that of PAP. The highest tensile strength of 47.57 MPa is associated with an energy consumption of 0.0302 kWh in Run 16. The lowest tensile strength, 36.31 MPa, occurs with an even higher energy consumption of 0.0334 kWh in Run 1. The highest energy consumption of 0.0368 kWh is observed in Run 3, producing a tensile strength of 42.79 MPa. On the other hand, the lowest energy consumption of 0.0194 kWh, recorded in Run 24, results in a tensile strength of 39.52 MPa.

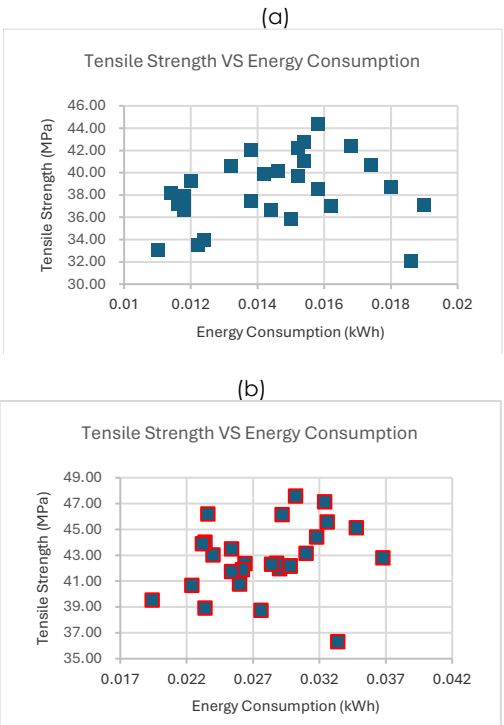

Figure 6 Tensile strength VS energy consumption data plots of: (a) PAP structure; (b) APA structure

3.5 Build time VS energy consumption

Figure 7 shows that the longest build time recorded in PAP structure is 482.0 seconds, which corresponds to the highest energy consumption of 0.019 kWh, observed in Run 3. Conversely, the shortest build time is 281.4 seconds, associated with the lowest energy consumption of 0.011 kWh, seen in Run 24.

In the case of the APA structure, a similar pattern emerges. The longest build time of 482.8 seconds is linked to the highest energy consumption of 0.0368 kWh, also in Run 3. The shortest build time of 271.6 seconds is associated with the lowest energy consumption of 0.0194 kWh, observed in Run 24.

The plot in Figure 7 shows that both structures demonstrate a consistent pattern where longer build times are directly correlated with higher energy consumption, while shorter build times require less energy. This relationship is evident in both the PAP and APA structures, suggesting that energy consumption is largely determined by the duration of the build process. The extended build times demand the 3D printer to operate for longer periods, which in turn consumes more power to maintain the necessary temperatures, motor functions, and overall operational processes required to complete the print.

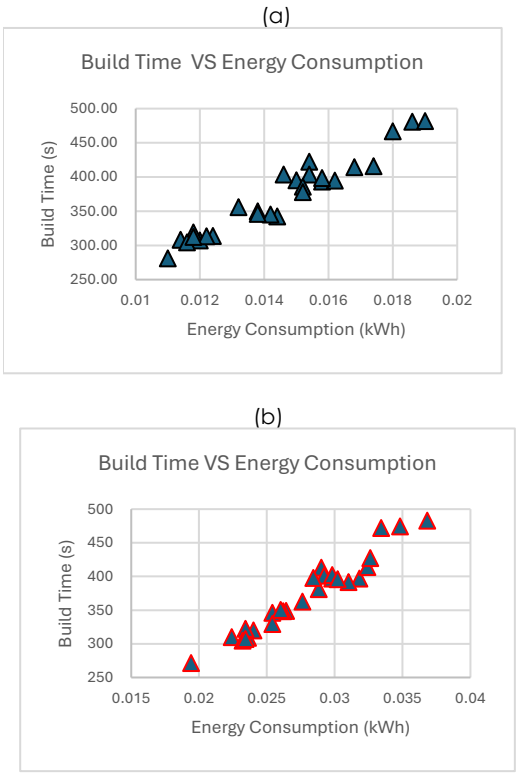

Figure 7 Build time VS energy consumption data plots of: (a) PAP structure; (b) APA structure

3.6 The effect of different levels of process parameters

From the Taguchi analysis in Figure 8, in the PAP structure, it is evident that for the majority of parameters (Layer Thickness, Raster Angle, Build Orientation, Raster Width, and Speed), the third level provides the optimal performance, followed by second level, and lastly first level. This indicates that for these parameters, the highest level offers the best efficiency in terms of build time (Layer Thickness of 0.33 mm, Raster Angle of 90°, Build Orientation of 45°, Raster Width of 0.578 mm, and Speed 60 mm/s). Conversely, for Infill Density, the lowest level is the most optimal (Infill Density of 80%), indicating that less dense infill patterns result in quicker build times. For Composition, the second level is the most efficient (Composition of 25/50/25), which may suggest a specific material composition balance that enhances build time efficiency.

Similar to the PAP structure, the parameters Layer Thickness, Raster Angle, Raster Width, and Speed show the same trend where third level is the most optimal, followed by second level, and lastly first level. This consistency reinforces the observation that higher levels of these parameters are generally beneficial for minimizing build time. Infill Density consistently shows that a lower density (Infill Density of 80%) results in faster build times across both structures. This is likely due to the reduced amount of material and shorter print paths required for less dense infill patterns. However, Build Orientation differs in the APA structure, with 00 being the most optimal level. This deviation suggests that the optimal build orientation may depend on the specific structure being printed, with different geometrical and structural considerations playing a role. Additionally, the Composition parameter shows a shift in the optimal level from 25/50/25 in PAP to 35/30/35 in APA. This variation indicates that the build time of material composition can be material-specific, potentially influenced by the melting properties.

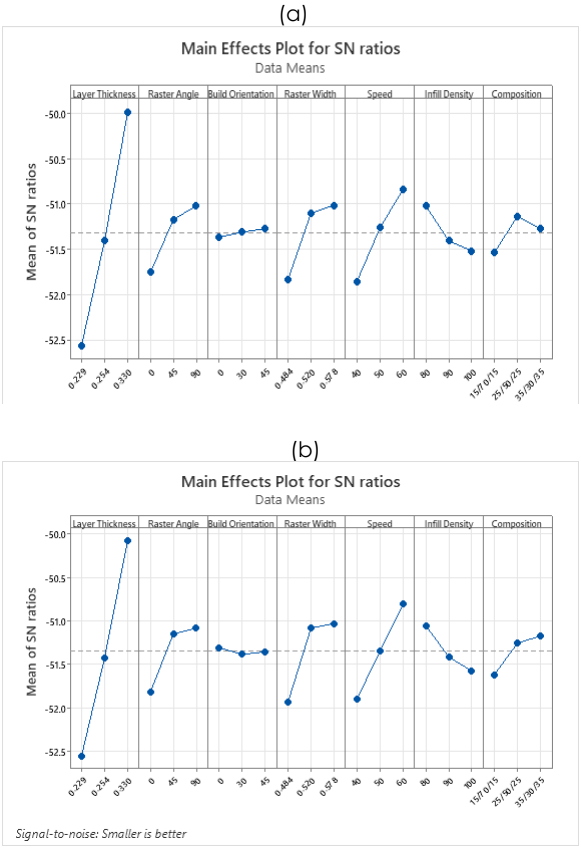

Figure 8 Taguchi analysis result of build time on: (a) PAP structure; (b) APA structure

On regards energy consumption, in the PAP structure (Figure 9(a)), it is evident that the third level is the most optimal for Layer Thickness, Raster Angle, Speed, and Composition, indicating that the highest level of these parameters reduces energy consumption the most. For Build Orientation, the first level is most efficient, suggesting that a specific orientation minimizes the energy required. The optimal Raster Width is 0.520 mm, which may reflect an ideal balance between the width of the raster and the energy used. Similarly, for Infill Density, the lowest level (Infill Density of 80%) is the most optimal, indicating that less dense infill patterns are more energy efficient.

The analysis for the APA structure (Figure 9(b)) shows a similar trend for Layer Thickness, Speed, and Composition, with the third level being the most optimal. However, the optimal Raster Angle in the APA structure is 45°, indicating a slight difference in how this parameter affects energy consumption compared to the PAP structure. For Build Orientation, 0° remains the most efficient, consistent with the PAP structure. The optimal Raster Width is also 0.520 mm, aligning with the findings for the PAP structure. The Infill Density parameter consistently shows that a lower density (Infill Density of 80%) results in lower energy consumption across both structures. This is likely due to the reduced material usage and less energy required for printing less dense infill patterns.

(a)

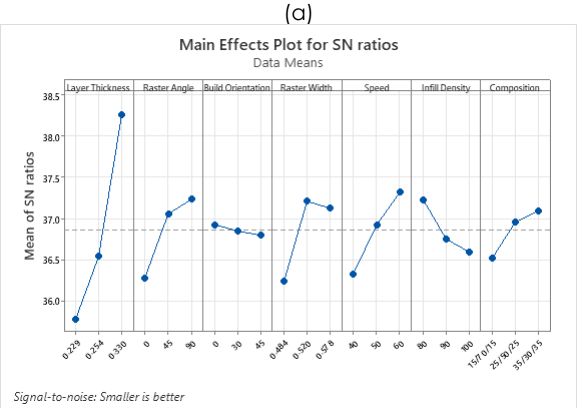

(b)

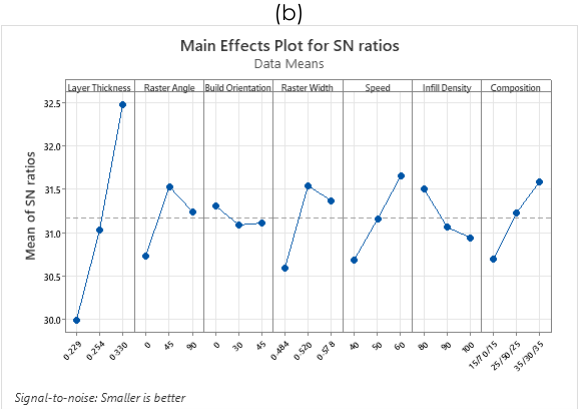

Figure 9 Taguchi analysis result of energy consumption on: (a) PAP structure; (b) APA structure

From the analysis results in Figure 10, it is evident that in PAP structure, the first level is the most optimal for Layer Thickness, Build Orientation, and Infill Density, indicating that the lowest level of these parameters provides the best dimensional accuracy. For Raster Angle, the third level is the most optimal (Raster Angle of 90°), suggesting that a specific angle achieves the best accuracy. Similarly, for Composition, the third level (35/30/35) is the most optimal. The optimal Raster Width is 0.520 mm, which may reflect a balance between the width of the raster and achieving dimensional precision. Finally, for Speed, the middle level (50 mm/s) is the most optimal.

The analysis for the APA structure shows a similar trend for Layer Thickness, Build Orientation, and Infill Density, with the first level being the most optimal. Both structures also find that Raster Width of 0.520 mm and Composition of 35/30/35 to be the most optimal, highlighting the importance of raster width and material composition in achieving dimensional accuracy. However, the optimal Raster Angle differs between the two structures, with 90° being optimal for PAP and 45° for APA. This suggests that the ideal raster angle may be structure-specific, potentially influenced by the geometry and specific accuracy requirements of each structure. For Speed, 60 mm/s is the most optimal, suggesting a different ideal speed for achieving accuracy in the APA structure.

(a)

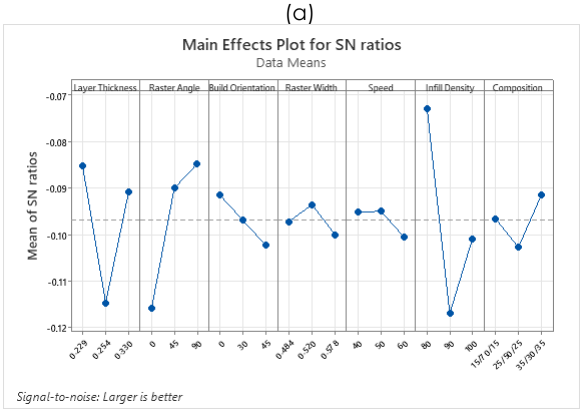

(b)

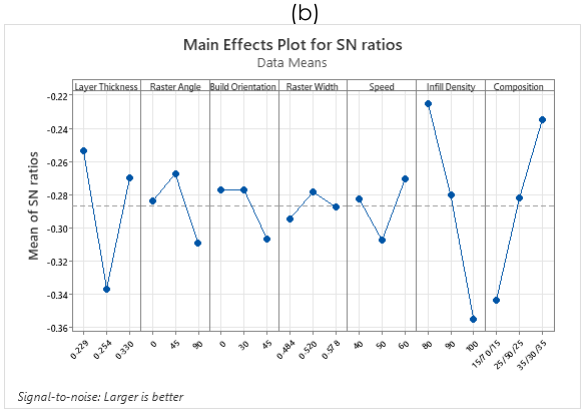

Figure 10 Taguchi analysis result of dimensional accuracy on: (a) PAP structure; (b) APA structure

In terms of tensile strength, in PAP structure (Figure 11(a)), the second level is the most optimal for Layer Thickness, Raster Width, Infill Density, and Composition, indicating that these middle levels provide the best tensile strength (Layer Thickness of 0.254 mm, Raster Width of 0.520 mm, Infill Density of 90%, and Composition of 25/50/25). For Raster Angle and Build Orientation, the third level is the most optimal (Raster Angle of 90°, Build Orientation of 45°), suggesting that the highest level of these parameters contributes to greater tensile strength. For Speed, the lowest level (40 mm/s) is the most optimal, indicating that slower print speeds result in better tensile strength.

The analysis for the APA structure (Figure 11(b)) shows a similar trend for Layer Thickness, Raster Width, and Infill Density, with the second level being the most optimal. However, the optimal Raster Angle in the APA structure is 45°, differing from the PAP structure where 90° was optimal. This suggests that the ideal raster angle may be structure-specific, influenced by the geometry and specific tensile strength requirements of each structure. Differ from PAP, Build Orientation of 0° is the most optimal in APA, indicating that different orientations are better suited for achieving maximum tensile strength in different structures. The optimal Speed is 50 mm/s, suggesting a moderate print speed is best for tensile strength in APA, contrasting with the PAP structure where 40 mm/s was optimal. Composition 25/50/25 is the most optimal in PAP, while in APA, 15/70/15 is the most optimal. This indicates that material composition's influence on tensile strength can be highly dependent on the specific structure.

(a)

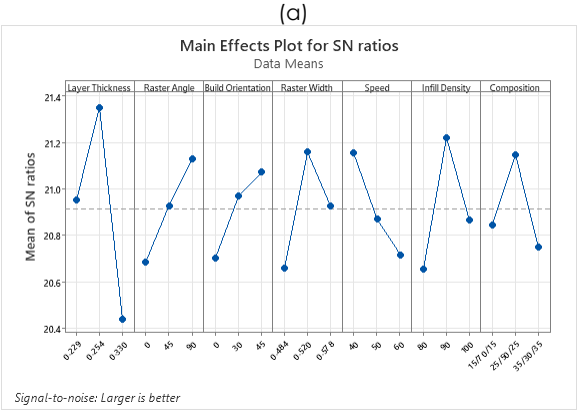

(b)

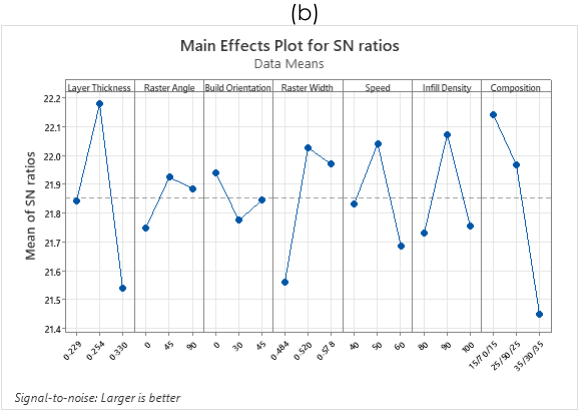

Figure 11 Taguchi analysis result of tensile strength on: (a) PAP structure; (b) APA structure

3.7 Significance of process parameters

The analysis of variance (ANOVA) in Table 7 highlights the P-values for seven different parameters concerning four outputs (Build Time, Energy Consumption, Dimensional Accuracy, and Tensile Strength). A P-value less than 0.05 indicates that the parameter has a significant influence on the output. The results are presented for two different structures, labelled as PAP and APA.

Table 7 P-value derived from ANOVA results

Parameters	Build time		Energy consumption		Dimensional accuracy		Tensile strength	
	PAP	APA	PAP	APA	PAP	APA	PAP	APA
Layer Thickness	0.000	0.000	0.000	0.593	0.025	0.003	0.000	0.000
Raster Angle	0.000	0.000	0.000	0.939	0.018	0.149	0.019	0.194
Build Orientation	0.000	0.096	0.666	1.000	0.565	0.252	0.045	0.189
Raster Width	0.000	0.000	0.000	0.908	0.807	0.719	0.002	0.000
Speed	0.000	0.000	0.000	0.916	0.807	0.199	0.005	0.002
Infill Density	0.000	0.000	0.000	0.978	0.003	0.000	0.000	0.000
Composition	0.000	0.000	0.000	0.985	0.532	0.000	0.050	0.000

For build time, all parameters significantly influence the output in the PAP structure, with P-values of 0.000 for each parameter, indicating a strong impact. In the APA structure, most parameters also show significant influence, except for Build Orientation, which has a P-value of 0.096. This suggests that while Build Orientation does not significantly affect build time in the APA structure, it is highly significant in the PAP structure.

Energy consumption shows significant results for all parameters in the PAP structure, except for Build Orientation, which has a P-value of 0.666. Conversely, in the APA structure, none of the parameters exhibit a significant influence, with P-values ranging from 0.593 to 1.000. This indicates that the PAP structure is more sensitive to variations in parameters regarding energy consumption compared to the APA structure. In general, a review by Vidakis *et al*. [61] indicates that energy consumption does not affected by build orientation. Additionally, in the APA (ABS-PLA-ABS) structure, the presence of more ABS layers (top and bottom) requires higher printing temperatures. This results in less variation in energy consumption, even when other printing parameters are altered. As a result, no printing parameter has a significant effect on energy consumption when printing the APA structure.

Dimensional accuracy is significantly influenced by Layer Thickness and Infill Density in both structures. In the PAP structure, these parameters have P-values of 0.025 and 0.003 respectively while in the APA structure is 0.003 and 0.000 respectively. While Raster Angle significantly affects dimensional accuracy in the PAP structure (P=0.018) but not in the APA structure (P=0.149). The Raster Angle affects how the printed material bonds to the previous layer, which in turn influences the adhesion between layers and impacts dimensional accuracy. ABS material has a slower cooling rate, which promotes better layer adhesion. Therefore, in the APA structure, which contains more

ABS layers, changes in the raster angle do not significantly affect adhesion. As a result, there is less variation in dimensional accuracy across different raster angles in the APA structure. On the other hand, composition shows a significant effect only in the APA structure (P=0.000). Generally, PLA have higher dimensional accuracy compared to ABS material, which have inherent shrinkage properties [19], [57]. In the PAP structure, PLA is used for the outer layers, which significantly influences the overall dimensional accuracy. As PLA has higher dimensional accuracy, the PAP structure tends to exhibit consistent and high dimensional accuracy, with less variation between specimens, even when printed with different composition percentages.

Tensile strength is significantly affected by most parameters in both structures. Layer Thickness, Raster Width, Speed, and Infill Density have consistently lower P-values than 0.05 in both PAP and APA structures. Specifically, Layer Thickness (P=0.000), Raster Width (P=0.002), Speed (P=0.005), and Infill Density (P=0.000) in the PAP structure, and Layer Thickness (P=0.000), Raster Width (P=0.000), Speed (P=0.002), and Infill Density (P=0.000) in the APA structure. Raster Angle and Build Orientation are significant in the PAP structure but not in the APA structure, with P-values of 0.019 and 0.045, respectively. Raster angle and build orientation affect how printed material bonds to the previous layer and how layers cool, influencing layer adhesion and mechanical properties like tensile strength. In the APA structure, which contains more ABS in the outer layers, the material's inherent adhesion properties reduce the impact of these factors on layer bonding. As ABS naturally promotes better adhesion, changes in raster angle and build orientation have a minimal effect on the tensile strength. Consequently, the tensile strength in the APA structure remains relatively consistent, even when varying the raster angle and build orientation. Meanwhile, Composition shows a significant influence on the APA structure (P=0.000) but not on the PAP structure (P=0.050). PLA generally has lower tensile strength than ABS, due to its material properties. In the PAP structure, PLA that is used as the outer layers is prone to breaking. Therefore, the use of PLA as the outer layers in PAP may result in less variation in tensile strength, even when the Composition percentages are changed.

3.8 Future Perspectives

Based on the experimental results, the APA sandwich structure exhibited superior tensile strength and Young's modulus, indicating its suitability for applications that demand high stiffness and resistance to deformation. Such performance characteristics make it ideal for components like electronic casings, lightweight structural elements, and interior parts of vehicles where mechanical rigidity is essential. In contrast, the PAP structure demonstrated better elongation at break, greater dimensional accuracy, improved energy efficiency, and more straightforward processing requirements. These attributes make it particularly advantageous for ultra-lightweight applications, including electronic components, drone airframes, and automotive interiors, where a balance between stiffness, damping capability, and controlled deformability is critical.

Despite the promising performance of both structures, the industrial application of these multimaterial sandwich configurations requires further investigation. In particular, understanding how these materials behave under real-world operational conditions will be crucial for their practical deployment.

Moreover, this study has several limitations that should be addressed in future research. For instance, the influence of process parameters on surface roughness has not been thoroughly examined. Additionally, the current analysis focuses only on the effects of printing parameters on tensile strength, dimensional accuracy, and energy efficiency. Future work should incorporate multi-objective optimization techniques using desirability functions or advanced metaheuristic algorithms such as NSGA-II and MOPSO. The objective will be to identify the most favourable combination of material compositions and process parameters that optimize multiple performance criteria, including mechanical strength, energy consumption, and print quality. Furthermore, sensitivity analysis and regression modelling will be employed to enhance the robustness of the optimization framework and to better understand the interdependencies among various parameters.

4.0 CONCLUSION

An investigation into the effects of various process parameters in multi-material FDM printing on energy consumption, build time, dimensional accuracy, and tensile strength has been conducted for two distinct sandwich structures: PLA/ABS/PLA (PAP) and ABS/PLA/ABS (APA). Generally, the APA structure exhibits superior tensile strength, but lower dimensional accuracy compared to the PAP structure. Despite variations in build time, the APA structure tends to consume more energy, even in instances where its build time is shorter than that of the PAP structure. This indicates that the material composition and structure type significantly influence energy consumption, beyond what is suggested by build time alone. When compared to existing literature, both structures outperform standard ABS and PLA in several key mechanical properties, highlighting the effectiveness of combining these materials in multi-material structures.

The data points analysis reveals that while there is a clear positive correlation between build time and energy consumption, there is no strong correlation between tensile strength and either build time or energy consumption, as the data points for tensile strength are scattered and show no clear linear trend. The analysis using ANOVA was further conducted to

identify which process parameters significantly affect energy consumption, build time, dimensional accuracy, and tensile strength.

The ANOVA analysis shows that the significance of the parameters varies between the PAP and APA structures. For the PAP structure, all parameters are significant for build time, whereas in the APA structure, Build Orientation is not significant. Regarding energy consumption, the PAP structure shows significant results for all parameters except Build Orientation, while the APA structure does not demonstrate this consistency. Dimensional accuracy in both structures is influenced by Layer Thickness and Infill Density, with additional significance observed for Raster Angle in the PAP structure and Composition in the APA structure. Tensile strength is similarly affected by multiple parameters across both structures, including Layer Thickness, Raster Width, Speed, and Infill Density. These findings underscore the critical role of method selection in additive manufacturing, as the choice of structure can significantly affect the importance of various parameters in achieving optimal print quality.

Acknowledgement

The authors would like to greatly appreciate support provided by the Centre for Higher Education Funding (BPPT), Indonesia Endowment Fund for Education (LPDP), and Department of Industrial Engineering, Universitas Sumatra Utara.

Conflicts of Interest

The authors declare that there is no conflict of interest regarding the publication of this paper

References

[1] Jiang, J. 2020. A Novel Fabrication Strategy for Additive Manufacturing Processes. *Journal of Cleaner Production.* 272: 122916. https://doi.org/10.1016/j.jclepro.2020.122916.

[2] Lacroix, R., R. W. Seifert, and A. Timonina-Farkas. 2021. Benefiting from Additive Manufacturing for Mass Customization across the Product Life Cycle. *Operations Research Perspectives.* 8: 100201. https://doi.org/10.1016/j.orp.2021.100201.

[3] Singh, G., A. Mehta, and H. Vasudev. 2024. Sustainability of Additive Manufacturing: A Comprehensive Review. *Progress in Additive Manufacturing*. https://doi.org/10.1007/s40964-024-00579-z.

[4] Nadagouda, M. N., M. Ginn, and V. Rastogi. 2020. A Review of 3D Printing Techniques for Environmental Applications. *Current Opinion in Chemical Engineering.* 28: 173–178. https://doi.org/10.1016/j.coche.2020.08.002.

[5] Javaid, M., A. Haleem, R. P. Singh, R. Suman, and S. Rab. 2021. Role of Additive Manufacturing Applications towards Environmental Sustainability. *Advanced Industrial and Engineering Polymer Research.* 4(4): 312–322. https://doi.org/10.1016/j.aiepr.2021.07.005.

[6] Embia, G., B. R. Moharana, A. Mohamed, K. Muduli, and N. B. Muhammad. 2023. 3D Printing Pathways for Sustainable Manufacturing. Springer International Publishing. https://doi.org/10.1007/978-3-031-20443-2_12.

[7] Prashar, G., H. Vasudev, and D. Bhuddhi. 2023. Additive Manufacturing: Expanding 3D Printing Horizon in Industry 4.0. *International Journal on Interactive Design and Manufacturing.* 17(5): 2221–2235. https://doi.org/10.1007/s12008-022-00956-4.

[8] Sartal, A., R. Bellas, A. M. Mejías, and A. García-Collado. 2020. The Sustainable Manufacturing Concept, Evolution and Opportunities within Industry 4.0: A Literature Review. *Advances in Mechanical Engineering.* 12(5). https://doi.org/10.1177/1687814020925232.

[9] Ingarao, G., and P. C. Priarone. 2020. A Comparative Assessment of Energy Demand and Life Cycle Costs for Additive- and Subtractive-Based Manufacturing Approaches. *Journal of Manufacturing Processes.* 56: 1219–1229. https://doi.org/10.1016/j.jmapro.2020.06.009.

[10] Kokare, S., J. P. Oliveira, and R. Godina. 2023. Life Cycle Assessment of Additive Manufacturing Processes: A Review. *Journal of Manufacturing Systems.* 68: 536–559. https://doi.org/10.1016/j.jmsy.2023.05.007.

[11] Somireddy, M., and A. Czekanski. 2020. Anisotropic Material Behavior of 3D Printed Composite Structures – Material Extrusion Additive Manufacturing. *Materials & Design.* 195: 108953. https://doi.org/10.1016/j.matdes.2020.108953.

[12] Kumar, R., M. Kumar, and J. S. Chohan. 2021. Material-Specific Properties and Applications of Additive Manufacturing Techniques: A Comprehensive Review. *Bulletin of Materials Science.* 44(3). https://doi.org/10.1007/s12034-021-02364-y.

[13] Sztorch, B., D. Brząkalski, D. Pakuła, M. Frydrych, Z. Špitalský, and R. E. Przekop. 2022. Natural and Synthetic Polymer Fillers for Applications in 3D Printing—FDM Technology Area. *Solids.* 3(3): 508–548. https://doi.org/10.3390/solids3030034.

[14] Alzyod, H., J. Takacs, and P. Ficzere. 2023. Improving Surface Smoothness in FDM Parts through Ironing Post-Processing. *Journal of Reinforced Plastics and Composites*. https://doi.org/10.1177/07316844231173059.

[15] Herianto, Mastrisiswadi, H., A. Nasution, and S. I. Atsani. 2023. Effect of Shot Peening Parameters on PLA Parts Manufactured with Fused Deposition Modeling. *Journal of Engineering and Technological Sciences.* 55(5): 513–523. https://doi.org/10.5614/j.eng.technol.sci.2023.55.5.1.

[16] Ngo, T. D., A. Kashani, G. Imbalzano, K. T. Q. Nguyen, and D. Hui. 2018. "Additive Manufacturing (3D Printing): A Review of Materials, Methods, Applications and Challenges. *Composites Part B: Engineering.* 143: 172–196. https://doi.org/10.1016/j.compositesb.2018.02.012.

[17] Stojković, J. R., *et al*. 2023. An Experimental Study on the Impact of Layer Height and Annealing Parameters on the Tensile Strength and Dimensional Accuracy of FDM 3D Printed Parts. *Materials.* 16(13). https://doi.org/10.3390/ma16134574.

[18] Wang, S., Y. Ma, Z. Deng, S. Zhang, and J. Cai. 2020. Effects of Fused Deposition Modeling Process Parameters on Tensile, Dynamic Mechanical Properties of 3D Printed Polylactic Acid Materials. *Polymer Testing.* 86: 106483. https://doi.org/10.1016/j.polymertesting.2020.106483.

[19] Milovanovic, A., *et al.* 2020. Comparative Analysis of Printing Parameters Effect on Mechanical Properties of Natural PLA and Advanced PLA-X Material. *Procedia Structural Integrity.* 28: 1963–1968. https://doi.org/10.1016/j.prostr.2020.11.019.

[20] Mishra, P. K., P. Senthil, S. Adarsh, and M. S. Anoop. 2021. An Investigation to Study the Combined Effect of Different Infill Pattern and Infill Density on the Impact Strength of 3D Printed Polylactic Acid Parts. *Composites Communications.* 24: 100605. https://doi.org/10.1016/j.coco.2020.100605.

[21] Srinivasan, R., W. Ruban, A. Deepanraj, R. Bhuvanesh, and T. Bhuvanesh. 2020. Effect on Infill Density on Mechanical Properties of PETG Part Fabricated by Fused Deposition Modelling. *Materials Today: Proceedings.* 27: 1838–1842. https://doi.org/10.1016/j.matpr.2020.03.797.

[22] Tanveer, M. Q., G. Mishra, S. Mishra, and R. Sharma. 2022. Effect of Infill Pattern and Infill Density on Mechanical Behaviour of FDM 3D Printed Parts—A Current Review. *Materials Today: Proceedings.* 62: 100–108. https://doi.org/10.1016/j.matpr.2022.02.310.

[23] Heidari-Rarani, M., N. Ezati, P. Sadeghi, and M. R. Badrossamay. 2022. Optimization of FDM Process Parameters for Tensile Properties of Polylactic Acid Specimens Using Taguchi Design of Experiment Method. *Journal of Thermoplastic Composite Materials.* 35(12): 2435–2452. https://doi.org/10.1177/0892705720964560.

[24] Srinivasan, R., T. Pridhar, L. S. Ramprasath, N. Sree Charan, and W. Ruban. 2020. Prediction of Tensile Strength in FDM Printed ABS Parts Using Response Surface Methodology (RSM). *Materials Today: Proceedings.* 27: 1827–1832. https://doi.org/10.1016/j.matpr.2020.03.788.

[25] Rasheed, A., *et al.* 2023. Experimental Investigation and Taguchi Optimization of FDM Process Parameters for the Enhancement of Tensile Properties of Bi-Layered Printed PLA-ABS. *Materials Research Express.* 10(9). https://doi.org/10.1088/2053-1591/acf1e7.

[26] Baca, D., and R. Ahmad. 2020. The Impact on the Mechanical Properties of Multi-Material Polymers Fabricated with a Single Mixing Nozzle and Multi-Nozzle Systems via Fused Deposition Modeling. *The International Journal of Advanced Manufacturing Technology*. 106(9–10): 4509–4520. https://doi.org/10.1007/s00170-020-04937-3.

[27] Yadav, D., D. Chhabra, R. Kumar Garg, A. Ahlawat, and A. Phogat. 2020. Optimization of FDM 3D Printing Process Parameters for Multi-Material Using Artificial Neural Network. *Materials Today: Proceedings.* 21: 1583–1591. https://doi.org/10.1016/j.matpr.2019.11.225.

[28] Peng, T. 2016. Analysis of Energy Utilization in 3D Printing Processes. *Procedia CIRP.* 40: 62–67. https://doi.org/10.1016/j.procir.2016.01.055.

[29] Ma, Z., *et al.* 2021. Energy Consumption Distribution and Optimization of Additive Manufacturing. *The International Journal of Advanced Manufacturing Technology*. 116(11–12): 3377–3390. https://doi.org/10.1007/s00170-021-07653-8.

[30] Yang, W., Y. Liu, J. Chen, Y. Chen, and E. Shang. 2024. Process-Based Modeling of Energy Consumption for Multi-Material FDM 3D Printing. *Journal of Intelligent Manufacturing and Special Equipment*. https://doi.org/10.1108/jimse-10-2023-0008.

[31] Camposeco-Negrete, C. 2020. Optimization of FDM Parameters for Improving Part Quality, Productivity and Sustainability of the Process Using Taguchi Methodology and Desirability Approach. *Progress in Additive Manufacturing.* 5(1): 59–65. https://doi.org/10.1007/s40964-020-00115-9.

[32] Lunetto, V., P. C. Priarone, M. Galati, and P. Minetola. 2020. On the Correlation between Process Parameters and Specific Energy Consumption in Fused Deposition Modelling. *Journal of Manufacturing Processes.* 56: 1039–1049. https://doi.org/10.1016/j.jmapro.2020.06.002.

[33] Enemuoh, E. U., S. Duginski, C. Feyen, and V. G. Menta. 2021. Effect of Process Parameters on Energy Consumption, Physical, and Mechanical Properties of Fused Deposition Modeling. *Polymers.* 13(15): 1–16. https://doi.org/10.3390/polym13152406.

[34] Giri, J., P. Shahane, S. Jachak, R. Chadge, and P. Giri. 2021. Optimization of FDM Process Parameters for Dual Extruder 3D Printer Using Artificial Neural Network. *Materials Today: Proceedings.* 43: 3242–3249. https://doi.org/10.1016/j.matpr.2021.01.899.

[35] Poonia, V., R. Kumar, R. Kulshrestha, and K. S. Sangwan. 2023. Optimization of Specific Energy, Scrap, and Surface Roughness in 3D Printing Using Integrated ANN-GA Approach. *Procedia CIRP*. 116: 324–329. https://doi.org/10.1016/j.procir.2023.02.055.

[36] Rojek, I., D. Mikołajewski, E. Dostatni, and M. Macko. 2020. AI-Optimized Technological Aspects of the Material Used in 3D Printing Processes for Selected Medical Applications. *Materials.* 13(23): 1–19. https://doi.org/10.3390/ma13235437.

[37] Fountas, N. A., J. D. Kechagias, D. E. Manolakos, and N. M. Vaxevanidis. 2020. Single and Multi-Objective Optimization of FDM-Based Additive Manufacturing Using Metaheuristic Algorithms. *Procedia Manufacturing.* 51: 740–747. https://doi.org/10.1016/j.promfg.2020.10.104.

[38] Panda, S. K., S. Padhee, A. K. Sood, and S. S. Mahapatra. 2009. Optimization of Fused Deposition Modelling (FDM) Process Parameters Using Bacterial Foraging Technique. *Intelligent Information Management.* 1(2): 89–97. https://doi.org/10.4236/iim.2009.12014.

[39] Sood, A. K., R. K. Ohdar, and S. S. Mahapatra. 2010. Parametric Appraisal of Mechanical Property of Fused Deposition Modelling Processed Parts. *Materials & Design.* 31(1): 287–295. https://doi.org/10.1016/j.matdes.2009.06.016.

[40] Srivastava, M., S. Rathee, S. Maheshwari, and T. K. Kundra. 2018. Multi-Objective Optimisation of Fused Deposition Modelling Process Parameters Using RSM and Fuzzy Logic for Build Time and Support Material. *International Journal of Rapid Manufacturing.* 7(1): 25–42. https://doi.org/10.1504/IJRAPIDM.2018.089727.

[41] Mohamed, O. A., S. H. Masood, J. L. Bhowmik, M. Nikzad, and J. Azadmanjiri. 2016. Effect of Process Parameters on Dynamic Mechanical Performance of FDM PC/ABS Printed Parts through Design of Experiment. *Journal of Materials Engineering and Performance.* 25(7): 2922–2935. https://doi.org/10.1007/s11665-016-2157-6.

[42] Liu, X., M. Zhang, S. Li, L. Si, J. Peng, and Y. Hu. 2017. Mechanical Property Parametric Appraisal of Fused Deposition Modeling Parts Based on the Gray Taguchi Method. *The International Journal of Advanced Manufacturing Technology.* 89(5): 2387–2397. https://doi.org/10.1007/s00170-016-9263-3.

[43] Aihemaiti, P., H. Jiang, W. Aiyiti, and A. Kasimu. 2021. Optimization of 3D Printing Parameters of Biodegradable Polylactic Acid/Hydroxyapatite Composite Bone Plates. *International Journal of Bioprinting.* 8(1): 490. https://doi.org/10.18063/ijb.v8i1.490.

[44] Torres, J., M. Cole, A. Owji, Z. DeMastry, and A. P. Gordon. 2016. An Approach for Mechanical Property Optimization of Fused Deposition Modeling with Polylactic Acid via Design of Experiments. *Rapid Prototyping Journal.* 22(2): 387–404. https://doi.org/10.1108/RPJ-07-2014-0083.

[45] De Bernardez, L., G. Campana, M. Mele, J. Sanguineti, C. Sandre, and S. M. Mur. 2023. Effects of Infill Patterns on Part Performances and Energy Consumption in Acrylonitrile Butadiene Styrene Fused Filament Fabrication via Industrial-Grade Machine. *Progress in Additive Manufacturing.* 8(2): 117–129. https://doi.org/10.1007/s40964-022-00316-4.

[46] Lopez, D. M. B., and R. Ahmad. 2020. Tensile Mechanical Behaviour of Multi-Polymer Sandwich Structures via Fused Deposition Modelling. *Polymers.* 12(3). https://doi.org/10.3390/polym12030651.

[47] Torres, J., J. Cotelo, J. Karl, and A. P. Gordon. 2015. Mechanical Property Optimization of FDM PLA in Shear with Multiple Objectives. *JOM.* 67(5): 1183–1193. https://doi.org/10.1007/s11837-015-1367-y.

[48] Abeykoon, C., P. Sri-Amphorn, and A. Fernando. 2020. Optimization of Fused Deposition Modeling Parameters for Improved PLA and ABS 3D Printed Structures. *International Journal of Lightweight Materials and Manufacture.* 3(3): 284–297. https://doi.org/10.1016/j.ijlmm.2020.03.003.

[49] V-Niño, E. D., A. Díaz Lantada, E. Mejía Ospino, A. Santos, R. Cabanzo Hernández, and J. L. Endrino. 2024. 3D Printed Polymer-Matrix Loaded with Graphene Oxide. *Materials Letters.* 372: 137012. https://doi.org/10.1016/j.matlet.2024.137012.

[50] Braconnier, D. J., R. E. Jensen, and A. M. Peterson. 2020. Processing Parameter Correlations in Material Extrusion Additive Manufacturing. *Additive Manufacturing.* 31: 100924. https://doi.org/10.1016/j.addma.2019.100924.

[51] Saeed, S., A. Eltahir, R. Gomaa, and Ç. Yilmaz. 2024. Effect of Strain Rate on the Tensile Properties of 3D-Printed PLA Specimens with Fused Deposition Modelling. *Journal of Aerospace and Mechanical Engineering.* 5: 37–46. https://doi.org/10.14744/ytu.jame.2024.00006.

[52] Pop, S. I., M. Dudescu, L. R. Contac, and R. V. Pop. 2023. Evaluation of the Tensile Properties of Polished and Unpolished 3D SLA- and DLP-Printed Specimens Used for Surgical Guides Fabrication. *Acta Stomatologica Marisiensis Journal.* 6(1): 14–21. https://doi.org/10.2478/asmj-2023-0003.

[53] De Bernardez, L., G. Campana, M. Mele, J. Sanguineti, C. Sandre, and S. M. Mur. 2023. Effects of Infill Patterns on Part Performances and Energy Consumption in Acrylonitrile Butadiene Styrene Fused Filament Fabrication via Industrial-Grade Machine. *Progress in Additive Manufacturing.* 8(2): 117–129. https://doi.org/10.1007/s40964-022-00316-4.

[54] Fountas, N. A., J. D. Kechagias, D. E. Manolakos, and N. M. Vaxevanidis. 2020. Single and Multi-Objective Optimization of FDM-Based Additive Manufacturing Using Metaheuristic Algorithms. *Procedia Manufacturing.* 51: 740–747. https://doi.org/10.1016/j.promfg.2020.10.104.

[55] Kam, M., A. Ipekçi, and Ş. Şengül. 2022. Taguchi Optimization of Fused Deposition Modeling Process Parameters on Mechanical Characteristics of PLA+ Filament Material. *Scientia Iranica.* 29(1B): 79–89. https://doi.org/10.24200/sci.2021.57012.5020.

[56] Kananathan, J., K. Rajan, M. Samykano, K. Kadirgama, K. Moorthy, and M. M. Rahman. 2023. Preliminary Tensile Investigation of FDM Printed PLA/Coconut Wood Composite. In *Technological Advancement in Instrumentation & Human Engineering*, edited by M. H. A. Hassan, M. H. Zohari, K. Kadirgama, N. A. N. Mohamed, and A. Aziz, 339–350. Singapore: Springer Nature Singapore.

[57] Milde, J., R. Hrušecký, R. Zaujec, L. Morovic, and A. Görög. 2017. Research of ABS and PLA Materials in the Process of Fused Deposition Modeling Method. *Annals of DAAAM & Proceedings of the International DAAAM Symposium*. 812–820. https://doi.org/10.2507/28th.daaam.proceedings.114.

[58] Alafaghani, A., A. Qattawi, B. Alrawi, and A. Guzman. 2017. Experimental Optimization of Fused Deposition Modelling Processing Parameters: A Design-for-Manufacturing Approach. *Procedia Manufacturing.* 10: 791–803. https://doi.org/10.1016/j.promfg.2017.07.079.

[59] Zharylkassyn, B., A. Perveen, and D. Talamona. 2021. Effect of Process Parameters and Materials on the Dimensional Accuracy of FDM Parts. *Materials Today: Proceedings.* 44: 1307–1311. https://doi.org/10.1016/j.matpr.2020.11.332.

[60] Zohdi, N., and R. C. Yang. 2021. Material Anisotropy in Additively Manufactured Polymers and Polymer Composites: A Review. *Polymers.* 13(19): 3368. https://doi.org/10.3390/polym13193368.

[61] Vidakis, N., J. D. Kechagias, M. Petousis, F. Vakouftsi, and N. Mountakis. 2023. The Effects of FFF 3D Printing Parameters on Energy Consumption. *Materials and Manufacturing Processes.* 38 (8): 915–932. https://doi.org/10.1080/10426914.2022.2105882.